HHS Public Access

Author manuscript

J Micromech Microeng. Author manuscript; available in PMC 2015 October 30.

Published in final edited form as:

J Micromech Microeng. 2013 ; 23(2): 025006–. doi:10.1088/0960-1317/23/2/025006.

Micromachined silicon acoustic delay lines for ultrasound applications

Cheng-Chung Chang[1], **Young Cho**[1], **Lihong Wang**[2], and **Jun Zou**[1]

Lihong Wang: junzou@ece.tamu.edu

[1]Department of Electrical and Computer Engineering, Texas A&M University, College Station, TX 77843, USA

[2]Department of Biomedical Engineering, Washington University in St. Louis, St. Louis, MO 63130, USA

Abstract

In this paper, we present the design, fabrication and testing of novel micromachined silicon-based acoustic delay lines. The acoustic properties of different silicon delay line structures have been characterized. Based on the experiment results, two different acoustic delay line systems (parallel and serial) have been successfully demonstrated to create controlled time delays in multiple channels of ultrasound signals. The time-delayed ultrasound signals are received with a single-element ultrasound transducer in a time-serial manner. This unique capability could be used to merge multiple signal channels, thereby enabling new ultrasound receiver designs with potentially less complexity and lower cost.

1. Introduction

Ultrasound transducer arrays have been widely used in ultrasound and photoacoustic imaging [1]. In either case, the transducer array receives the incoming ultrasound waves from the source point(s), and the received signals are processed by the data acquisition (DAQ) electronics simultaneously (figure 1). To achieve high imaging resolution and speed, large high-frequency transducer arrays and complex DAQ electronics will be needed [2, 3]. As a result, the entire ultrasound imaging system could become costly.

To address this issue, a new ultrasound receiving system design using acoustic time delay was demonstrated [4]. As shown in figure 2*(a)*, a series of acoustic delay line detectors are used to replace the transducer elements. Each delay line receives the acoustic wave (figure 2*(b)*) and introduces proper delay time for the signal to reach the other end (figure 2*(c)*), where a single transducer is connected to serially receive the time-delayed signals (figure 2*(d)*). The delay line system converts multi-channel parallel signals into single-channel serial signals and therefore requires fewer transducer elements and DAQ channels. It could be a more economical new approach for ultrasound receiving system design.

Previously, liquid mercury delay lines [5] and solid delay lines based on quartz rods[6], metal wires [7] and optical fibers [8] were used in a number of applications [9]. The acoustic propagation in these delay lines were also studied [10-12]. Among them, optical-fiber delay lines are most desirable due to their low acoustic loss, small dimensions, and abundance of

materials. However, because of the high acoustic velocity of quartz (e.g., ~6000 m/sec), the length of the optical-fiber delay lines need to be very large to provide sufficient delay time [4]. The plastic jacket layer would cause extra attenuation and distortion of the acoustic signals. In addition, the manual assembly and alignment of the optical fibers are very tedious and inaccurate. To address these issues, we report the development of new micromachined silicon acoustic delay lines, which capitalize upon the extremely low acoustic loss of single-crystalline silicon and the micro scale precision of micromachining process. Compared with the optical-fiber delay lines, the micromachined silicon delay lines offer higher transmission efficiency, more compact and functional structures, easier assembly, and mass production. By using the silicon delay lines, two acoustic delay line systems (parallel and serial) have been successfully demonstrated to create controlled time delays in multiple channels of ultrasound signals, which allows their reception with a single-element transducer.

2. Design of silicon acoustic delay line

Silicon is considered as the delay line material for three reasons. First, it has extremely low attenuation in the MHz range (~10^{-4} dB/mm·MHz^2 @ 10 MHz) [13]. The dispersion of ultrasound wave propagation can be minimized with proper design [14]. Second, it is a mechanically strong material with excellent thermal stability. Third, it is compatible with well-developed microfabrication and micromachining technologies. Multiple delay line structures can be simultaneously fabricated with high precision in a compact space without tedious assembly process.

The dimension of the delay lines affects the transmission of the acoustic signal. To operate only in the lowest longitudinal mode, the dimension of a rectangular-shaped delay line should satisfy $(df/V_0) \ll 1$, where d is the width or thickness of the delay line (whichever is smaller), f is the frequency of the signal, and V_0 is the acoustic velocity of the delay line material [14]. For example, suppose the acoustic velocity in silicon is around 8430 m/s [15], the dimension for the single mode delay line should be much smaller than 3.7 mm for a 2.25 MHz center frequency wave transmission. In this work, all the fabricated delay line structures have a width of 500 μm and a thickness of 250 μm.

In the delay line system, each channel has a designated delay time, which is controlled by the travelling length of the signal. Two different layouts, parallel and serial, can be applied for silicon delay lines. In the parallel design, each channel carries one signal with a specific propagation path and delay. All the channels connect to the same transducer in a parallel fashion. Signal from each channel arrives at the transducer at different time (figure 3). Since the acoustic velocity of silicon is high, the delay lines need to be long to achieve sufficient delay time in each channel. To satisfy the length requirement and remain compact in size, each channel is made of multiple U-turns with different radius winding together. In the serial design, all channels merge into the main channel at different locations with Y-shaped junctions. The delay time is controlled by the travelling length in the main channel (figure 4).

3. Materials and methods

To ensure a good design of the silicon-based delay lines, the acoustic properties of silicon, such as the velocity and attenuation, were first characterized. In the second step, the wave propagation in the three fundamental building-block structures (straight line, U-turn, and Y-junction) in the parallel and serial delay lines were simulated and experimentally tested.

3.1. Delay line structure fabrication

The delay line structures were fabricated using 250-μm-thick 4-inch {100} single-crystalline silicon wafers. The silicon wafer was first coated with a 300 nm thick aluminum layer using e-beam evaporation. The aluminum layer was patterned using photolithography, which served as a mask for silicon etching. The etching of the delay line structures was conducted using a cryogenic deep reactive ion etching (RIE) process on a Plasmalab® 100 RIE system (Oxford Instruments, Oxfordshire, UK). The cryogenic etching process can provide high etch rate and vertical sidewall profile [16]. The silicon wafer was first glued on an aluminum-coated dummy wafer with Fomblin oil (Fomblin 06/6, Solvay Plastics, Brussels, Belgium). The whole sample was later clamped on the chuck cooled down to -120° Celsius by using liquid nitrogen with liquid helium backing between the dummy wafer and the chuck. The RIE etching was conducted for 60 minutes to completely etch through the silicon wafer. After etching, the delay line structures were carefully detached from the etched silicon wafer.

3.2. Characterization setup

As shown in figure 5, the silicon samples are supported by acrylic plates with small holding structures to minimize signal leakage. The acrylic plates together with the sample and a longitudinal wave transducer are fixed on a three axis translation stage. The acoustic wave signal is directly generated in silicon through the photoacoustic effect [17]. Photoacoustic effect is the generation of acoustic wave by pulsed light excitation. The material absorbs light energy and heats up, and the sudden thermal expansion creates pressure waves that radiate away from the excitation spot. The pressure wave involves surface acoustic wave and longitudinal and shear waves that propagate within the silicon delay line [18]. Using photoacoustic setup, the acoustic wave can be generated at any points on the sample by changing the location of the laser focal point. The small laser focal spot is particularly suitable for acoustic wave excitation in sub-millimeter structures. Nanosecond laser pulses with 1064 nm wavelength are delivered onto the sample from a Nd: YAG laser (Quanta-Ray Pro-200, Newport Corporation, Irvine, CA, USA) with a 10 Hz repetition rate and 10 nanosecond pulse width. A shutter controlled by the trigger in the laser system is used to allow single pulse excitation. The laser is attenuated by a half-wavelength wave plate, a dielectric polarizer, two filters, and focused by an objective lens to form a beam spot of 10 μm in diameter. The focused pulse energy is 280 J/mm^2 with 10 percent variance. Silicon sample absorbs light energy and induces a pressure wave in all directions. The pressure wave propagates along the silicon delay line structure and only the longitudinal component of the wave is detected by an ultrasound transducer with a 2.25 MHz center frequency (V105, Olympus NDT, Waltham, MA, USA). The ends of the silicon are polished to create flat contact surfaces and mineral oil is applied at the silicon-transducer interface to improve

contact and coupling efficiency. The received signal is amplified by the pulser-receiver unit (5072-PR, Olympus NDT, Waltham, MA, USA) with 1 MHz high pass filter and 10 MHz low pass filter. The acoustic signal and the laser trigger signal are displayed on an oscilloscope. The data are collected for three times and averaged for each measurement.

3.3. Simulation setup

The acoustic wave propagation inside the silicon delay line is investigated using ultrasound simulation software (Wave2000 Plus, Cyberlogic, New York, NY, USA). In the 2-dimension simulation model, the silicon delay line sample is placed inside an air cavity with infinite boundary conditions. A 10 μm diameter point source is placed inside the delay line to simulate the wave generated from the laser spot. A receiving transducer unit is set on the other end of the delay line to follow the experimental settings.

4. Simulation and experiment results

4.1. Acoustic properties: attenuation and velocity

A 7-cm-long straight silicon delay lines etched along the <1 1 0> crystal direction was used to measure the acoustic attenuation and velocity (figure 6*(a)*). Laser light was focused on the delay line at a particular distance away from the transducer (figure 6*(b)*). The generated acoustic wave propagates in two directions. The wave traveling toward the transducer is received first, and the wave traveling away from the transducer is reflected on the other end and reaches the transducer at a later time. To avoid the reflected signal to mix with the first signal, the measuring locations were kept away from both ends of the delay line. Signals from eight different points with ~5 mm intervals were measured along the delay line. The received signals were used to determine the acoustic velocity and attenuation. The velocity can be calculated based on the ratio of the travelling length and arrival time. The averaged velocity for a straight delay line is determined to be ~8454m/s (figure 6*(c)*). The attenuation can be determined by measuring the peak to peak amplitude change of the signal. From the simulation (figure 6*(d)*) and experimental results (figure 6*(e)*), there is no significant change in amplitude as the travelling length increases. The small variation in the experiment results is due to the tolerance of laser power and the difference in surface condition at the focus location. These results imply that at 2.25 MHz, the acoustic attenuation is extremely low and can be negligible.

4.2. Propagation in U-turn structures with different bending radii of curvature

As shown in figure 7*(a)*, U-turn structures with six different bending radii of curvature were attached to the receiving transducer. Each U-turn structure consists of two straight portions (with lengths of 3 cm and 1 cm) connected by a 180° round portion. The laser focal spot was position on the two junction points (i.e., points A and B in figure 7*(b)*) between the straight portion and the bending portion, respectively. The first-arrival signal from point A only travels in the 3-cm-long straight portion before reaching the transducer. The first-arrival signal from point B travels in both the curved and straight portion. Since the attenuation of silicon is very low at 2.25 MHz, any difference between these two signals is mainly due to the bending portion. Therefore, the insertion loss of the bending portion can be estimated by comparing the peak-to-peak amplitude of these two signals. As shown in the simulation

(figure 7*(c)*) and experimental results (figure 7*(d)*), the amplitude ratio decreases as the bending radius decreases. The reduction is due to the mode conversion and direct reflection of the wave. As longitudinal wave hit on the wall of the delay line with an angle, the wave will go through reflection. Part of the reflected wave will remain in longitudinal mode and part of the wave will go through mode conversion and become transverse mode, which cannot be effectively detected by the longitudinal mode transducer. In addition, when the bending radius is small, some of the waves will be reflected back and never reach the transducer. It is observed that the experimental results are smaller than the simulation results. This can be explained by the imperfectness of the side wall reflection surface. While the simulation assumes smooth surface with specular reflection at the delay line side wall, the delay line in the experiment goes through diffuse reflection from the etched rough side wall surface. Therefore, the acoustic wave is less probable to pass the bending and reach the receiving transducer on the other end. It is also noticed that the signal wave form is similar to the signal from a straight delay line and no signal distortion being observed. However, after receiving the first peak and the reflected peak from the other end, the signal becomes more distorted as the radius decreases.

4.3. Propagation in Y-junction structures with different interception angles

Six Y-junction structures with cross angles ranging from 5 degrees to 30 degrees (with a 5-degree increment) (figure 8*(a)*) were tested. Each structure has a 4-cm-long straight line with a 3-cm-long branch. The intersection point is located 1 cm away from the transducer (figure 8*(b)*). The laser focal spot was positioned at three points one at a time to determine the insertion loss at the junction. Signal generated from point A does not go through the junction and is used as the reference signal. Signal from point B comes from the branch and enters the straight line through the junction. Signal from point C is from the straight line and passes the junction. By comparing the peak-to-peak amplitude of the signals from the three points, the insertion loss of the straight and branch parts at the junction can be estimated. As shown in the simulation (figure 8*(c)*) and experimental results (figure 8*(d)*), at a small cross angle, the insertion loss is not significantly affected by the change of the angle. Signals coming from the straight part or the branch do not have much difference. The average insertion loss of the Y-junction is around 20%, which is due to the wave leakage and reflection into the other branch.

4.4. Comparison of signal shape from different structures

The typical acoustic pulse shape and spectrum of the first received signal are compared to investigate the structural effect on wave form in each structure (figure 9). All signals appear to have similar pulse shapes, and the pulse duration remains within 1 μs. The power spectrum shows that most signals are below 5 MHz, which matches well with the frequency response of the transducer.

Our experimental results show that the difference in structure of the delay line does not cause significant signal distortion, but only changes in amplitude. By carefully design the length and structure, acoustic signal can have a designated time delay with a distinguishable pulse shape. As a result, the straight, U-turn, and y-junction structures can be applied in the design for serial and parallel delay lines.

5. Multi-channel serial and parallel delay lines

A 4-channel serial delay line and a 4-channel parallel delay line were designed, fabricated and tested. The serial delay line has four inputs and one output, which consists of straight lines, U-turns with 4 mm radius, and 30- degree Y-junctions (figure 10). The parallel delay line has four inputs and four outputs. Each channel consists of a multiple-turn spiral structure with a minimal radius of 2.5 mm (figure 11). The serial and parallel delay lines were tested using a two-port ultrasound measurement setup (figure 12). The delay lines were fixed on an acrylic holder with its inputs and outputs polished. A pulser-receiver unit was used to generate a driving voltage pulse for a 2.25 MHz transmitting transducer (V106, Olympus NDT, Waltham, MA, USA). The four delay line inputs received the ultrasound pulse at the same time from the transmitting transducer. The four pulses travelled different length in the delay line and arrived at the outputs at different time. The receiving transducer captured the signals from the outputs, which were amplified by pulser-receiver unit. The signals were averaged 128 times and displayed on the oscilloscope.

Figure 13 shows the received signals from the serial and the parallel delay lines. Both delay line structures successfully achieved four time-delayed signals with approximately 7 μs interval between adjacent channels. It is observed that the signal amplitude in both designs decreases from channel 1 to channel 4. Since the attenuation in silicon is negligible, the loss is due to the delay line structure. In the serial delay line structure, the loss is from both the U-turns and Y-junctions. While in the parallel delay line structure, the loss is from the curve structures. Because the signal in longer channel goes though more U-turns and Y-junctions, it has a higher total insertion loss resulting in a smaller signal. Despite of the loss, signals from the delay line structures remain clear and distinctive.

6. Conclusion

In this work, we have successfully demonstrated micromachined silicon acoustic delay lines. The acoustic velocity, attenuation, and propagation through bending and junction structures have been simulated and characterized. True acoustic time delay has been demonstrated using 4-channel serial and parallel delay lines. Our experimental results show that with proper design and construction of the delay line structure, acoustic signals can be transmitted with minimal attenuation and distortion. With the addition of acoustic time delay, it is possible to receive multiple acoustic signals using one single-element transducer, followed by a single-channel of data acquisition electronics. We expect that the micromachined silicon delay lines can be applied to simplify the ultrasound receiver system architecture and reduce its costs, thereby helping to widen the applications of ultrasound imaging by enabling new modalities. To better enhance the imaging capability, a matching layer will be attached on the silicon delay line ends to improve the coupling efficiency of the signal. The delay line dimension and the transducer frequency used will also be optimized for the directivity effect. Our future work will investigate the high-frequency transmission and switching of the silicon delay lines to achieve highly functional and integrated reconfigurable delay line systems.

Acknowledgments

This work is supported in part through a grant from the National Science Foundation (CMMI-1131758) and National Institutes of Health (U54 CA136398). The authors would like to thank Dr. D. Voronine and Mr. K. Wang from the Department of Physics for their kindly assistance on the photoacoustics setup.

References

1. Wang LV. Tutorial on photoacoustic microscopy and computed tomography. IEEE J Sel Top Quant Electron. 2008; 14:171–9.
2. Gamelin J, Maurudis A, Aguirre A, Huang F, Guo PY, Wang LV, Zhu Q. A real-time photoacoustic tomography system for small animals. Opt Express. 2009; 17:10489–98. [PubMed: 19550444]
3. Song L, Kim C, Maslov K, Shung KK, Wang LHV. High-speed dynamic 3D photoacoustic imaging of sentinel lymph node in a murine model using an ultrasound array. Med Phys. 2009; 36:3724–9. [PubMed: 19746805]
4. Yapici MK, K C, Chang C-C, Jeon M, Guo Z, C X, Zou J, Wang LV. Parallel acoustic delay lines for photoacoustic tomography. J Biomed Opt. 2012 Submitted.
5. Auerbach IL, Eckert JP, Shaw RF, Sheppard CB. Mercury delay line memory using a pulse rate of several megacycles. Proc Inst Radio Eng. 1949; 37:855–61.
6. Arenberg DL. Ultrasonic solid delay lines. J Acoust Soc Am. 1948; 20:1–26.
7. Scarrott GG, Naylor R. Wire-type acoustic delay lines for digital storage. Proc of the IEE - Radio and Electron Eng B. 1956; 103:497–508.
8. Boyd GD, Coldren LA, Thurston RN. Acoustic clad fiber delay-lines. IEEE Trans Son Ultrason. 1977; 24:246–52.
9. Palfreeman JS. Acoustic delay lines— a survey of types and uses. Ultrasonics. 1965; 3:1–8.
10. May JE. Wire-type dispersive ultrasonic delay lines. IRE Trans Ultrason Eng. 1960; 7:44–52.
11. Meitzler AH. Ultrasonic delay lines for digital data storage. IRE Trans Ultraon Eng. 1961; 9:30–7.
12. Gibson RW. Solid ultrasonic delay lines. Ultrasonics. 1965; 3:49–61.
13. Auld, BA. Acoustic fields and waves in solids. Melbourne, Florida: Charles Krieger; 1991.
14. Meeker TR. Dispersive ultrasonic delay lines using the first longitudinal mode in a strip. IRE Trans Ultrason Eng. 1960; 7:53–8.
15. David, J.; C, N. Fundamentals and applications of ultrasonic waves. Montreal, Canada: CRC Press; 2002.
16. De Boer MJ, Gardeniers JGE, Jansen HV, Smulders E, Gilde MJ, Roelofs G, Sasserath JN, Elwenspoek M. Guidelines for etching silicon MEMS structures using fluorine high-density plasmas at cryogenic temperatures. J Microelectromech Syst. 2002; 11:385–401.
17. Rosencwaig A, Gersho A. Theory of the photoacoustic effect with solids. J Appl Phys. 1976; 47:64–9.
18. Aussel JD, Brun AL, Baboux JC. Generating acoustic waves by laser: theoretical and experimental study of the emission source. Ultrason. 1988; 26:245–55.

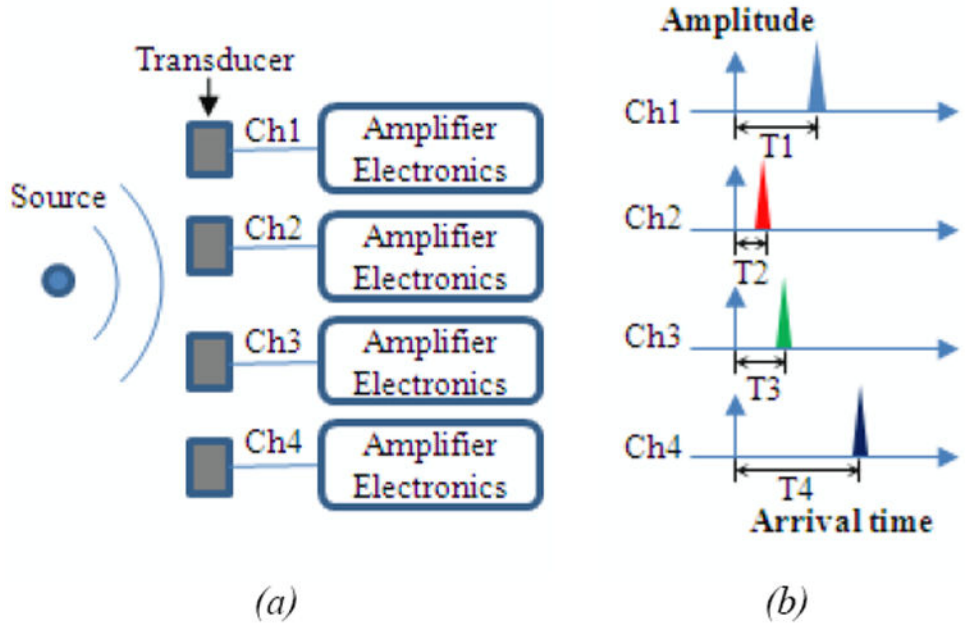

Figure 1.

Ultrasound transducer array system: *(a)* Transducer array setup; *(b)* Signals received by each transducer. The arrival time is determined by the travel distance and acoustic velocity in the medium.

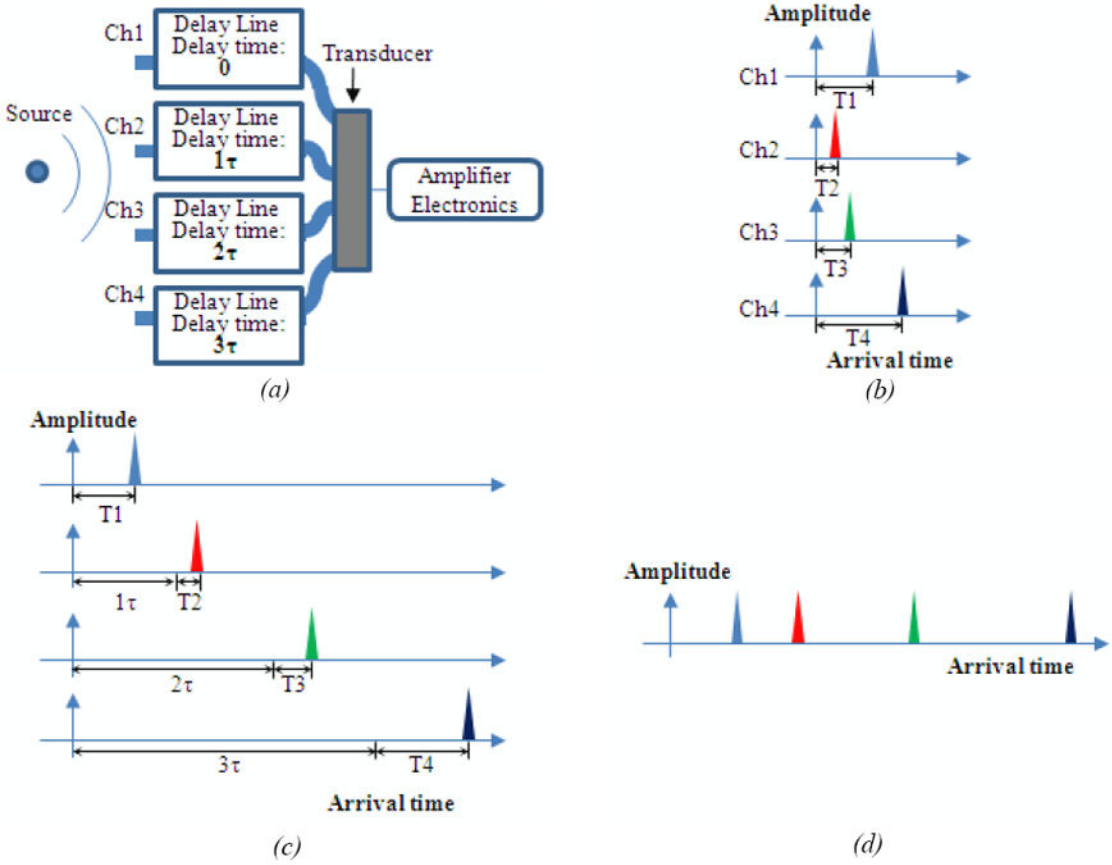

Figure 2.

Delay line receiving system: *(a)* Delay lines with single receiving transducer; *(b)* Ultrasound signals before entering the delay lines; *(c)* Ultrasound signals with proper delay time; and *(d)* Ultrasound signals received by the single transducer.

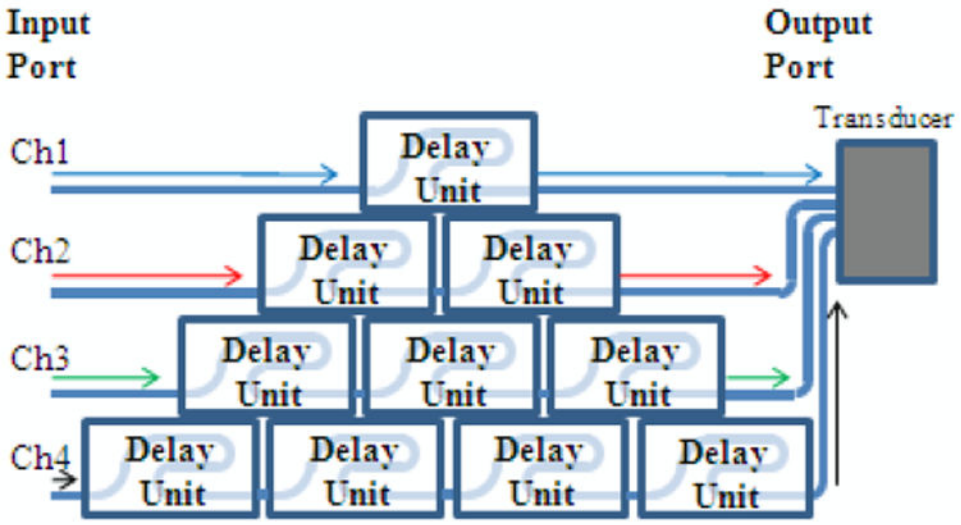

Figure 3.
Schematic of parallel delay lines.

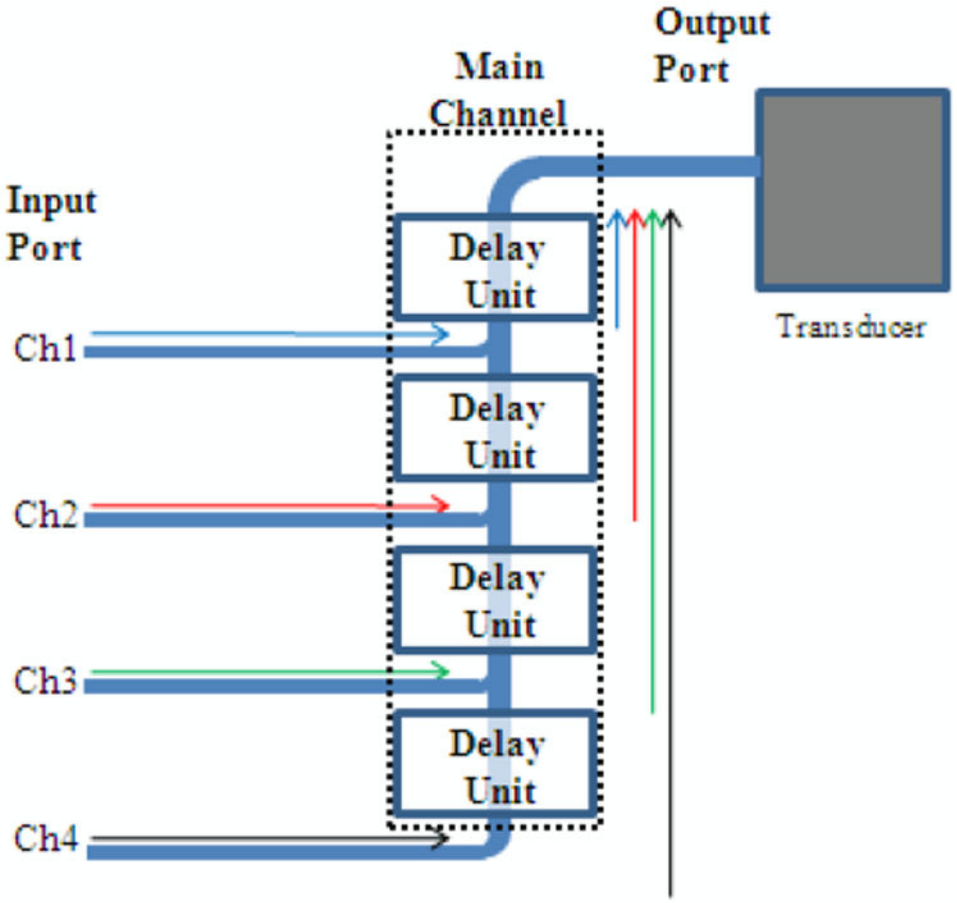

Figure 4.
Schematic of serial delay lines.

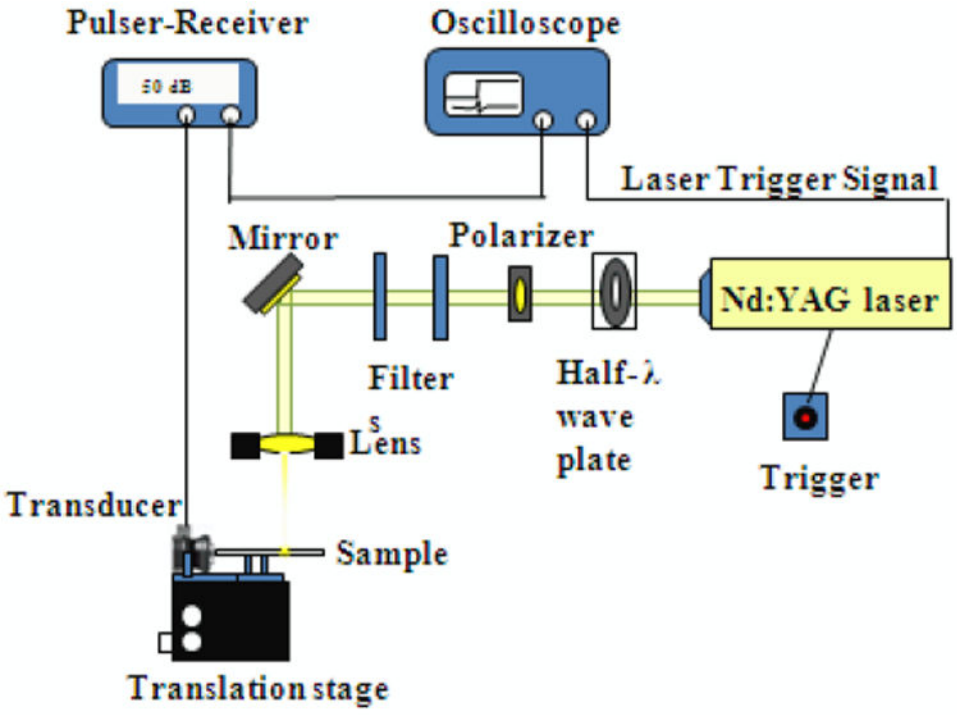

Figure 5.
Schematic of the photoacoustic excitation setup.

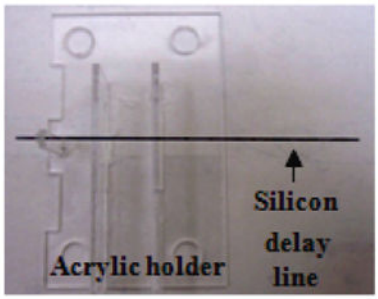

(a)

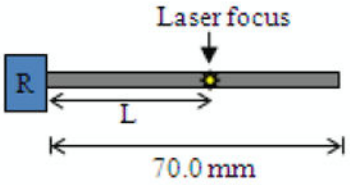

(b)

Length (mm)	Time (μs)	Velocity (m/s)
28.2	3.32	8494
33.9	3.86	8782
38.9	4.46	8722
44.5	5.26	8460
50.3	6.15	8179
54.9	6.3	8714
60.9	7.45	8174
66.0	8.14	8108
	Average= 8454 m/s	

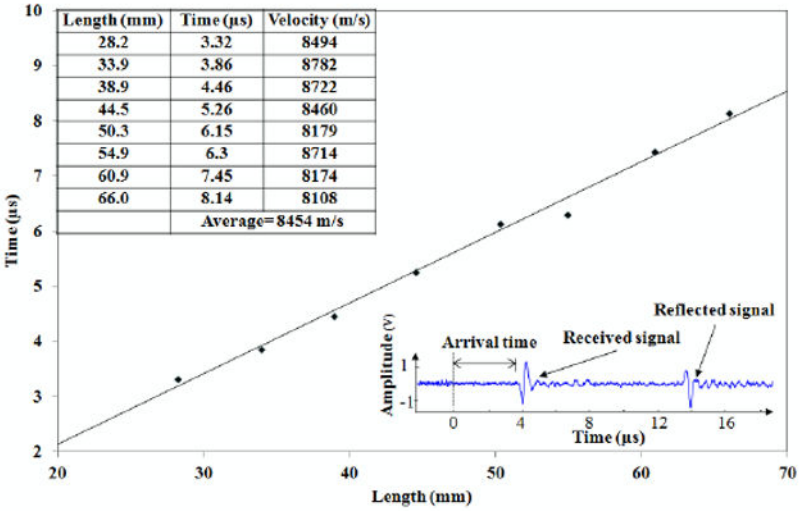

(c)

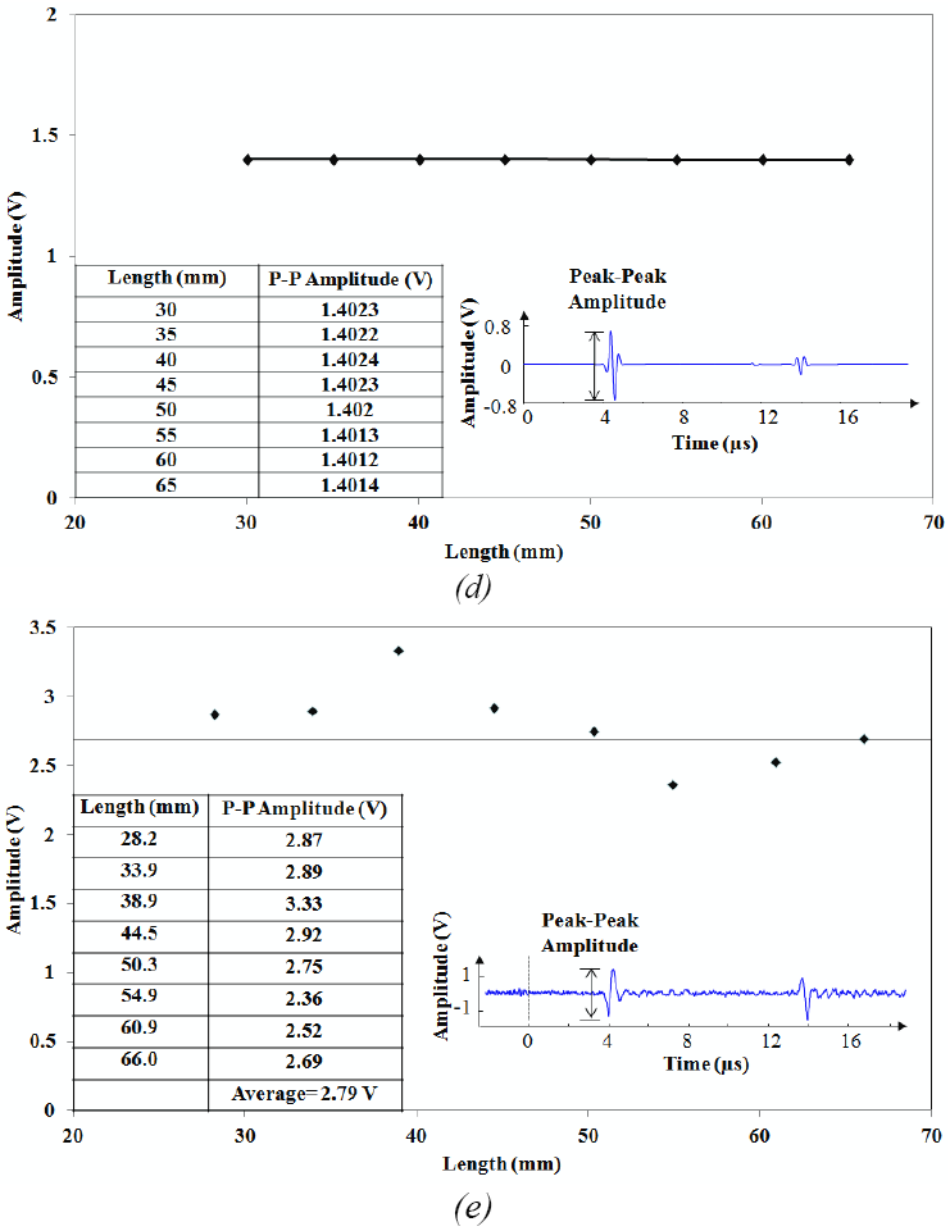

Figure 6.

Straight silicon delay line measurement. *(a)* Sample; *(b)* Measurement setup: Receive signal from focus points along the straight delay line. L: Traveling length (distance from the focal point to the transducer). R: Receiving transducer; *(c)* Plot of the arrival time versus traveling length. The average velocity in straight silicon delay line is ~8454 m/s. Inset: Representative signal shape from L: 28.2 mm; *(d)* Simulation results of signal peak–peak amplitude versus traveling length. Inset: Representative signal shape from L: 30 mm; and *(e)* Experimental results of signal peak–peak amplitude versus traveling length. Inset: Representative signal shape from L: 28.2 mm.

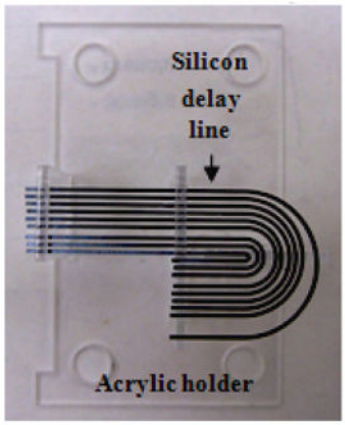

(a)

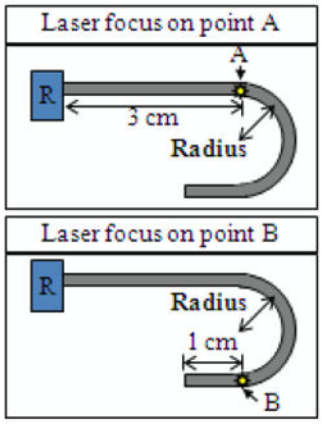

(b)

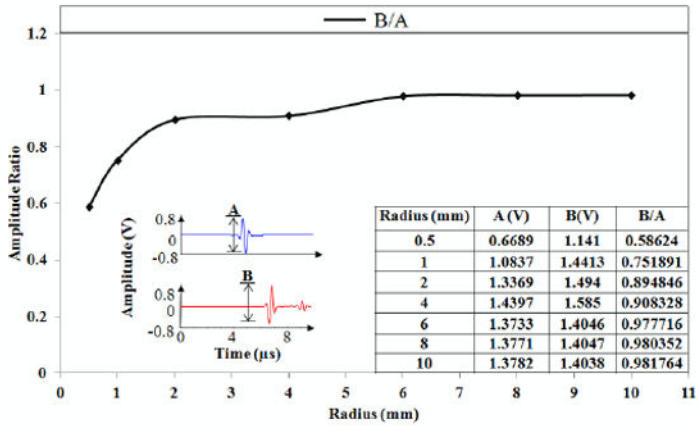

Radius (mm)	A (V)	B(V)	B/A
0.5	0.6689	1.141	0.58624
1	1.0837	1.4413	0.751891
2	1.3369	1.494	0.894846
4	1.4397	1.585	0.908328
6	1.3733	1.4046	0.977716
8	1.3771	1.4047	0.980352
10	1.3782	1.4038	0.981764

(c)

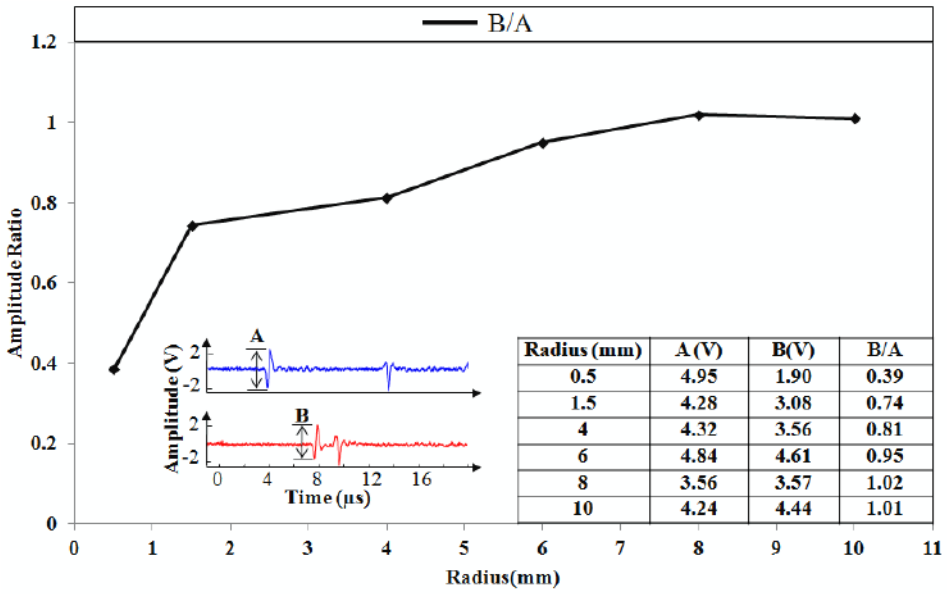

Radius (mm)	A (V)	B(V)	B/A
0.5	4.95	1.90	0.39
1.5	4.28	3.08	0.74
4	4.32	3.56	0.81
6	4.84	4.61	0.95
8	3.56	3.57	1.02
10	4.24	4.44	1.01

(d)

Figure 7.

U-turn structure measurement. *(a)* Sample; *(b)* Measurement setup: Receive signals from different focus points, A: without bending, B: with bending; *(c)* Simulation results of radius versus amplitude ratio. Inset: Representative signal shape from turning with 6 mm radius; and *(d)* Experimental result of radius versus amplitude ratio. Inset: Representative signal shape from turning with 6 mm radius.

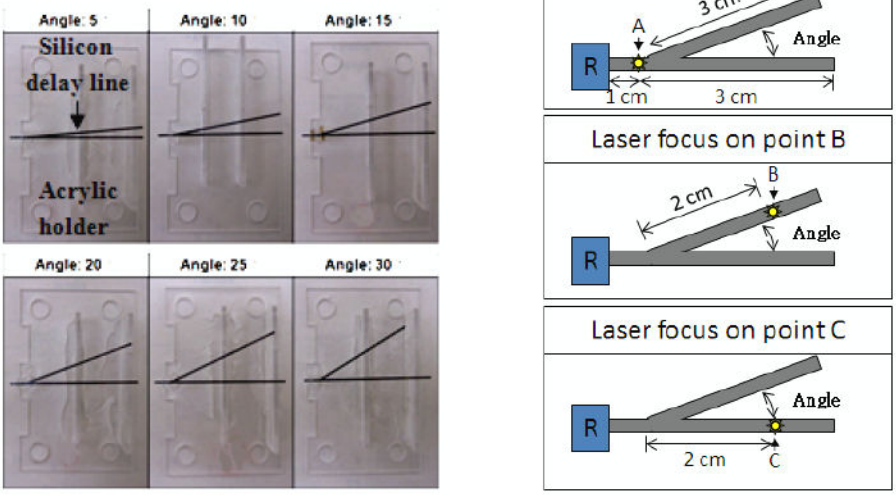

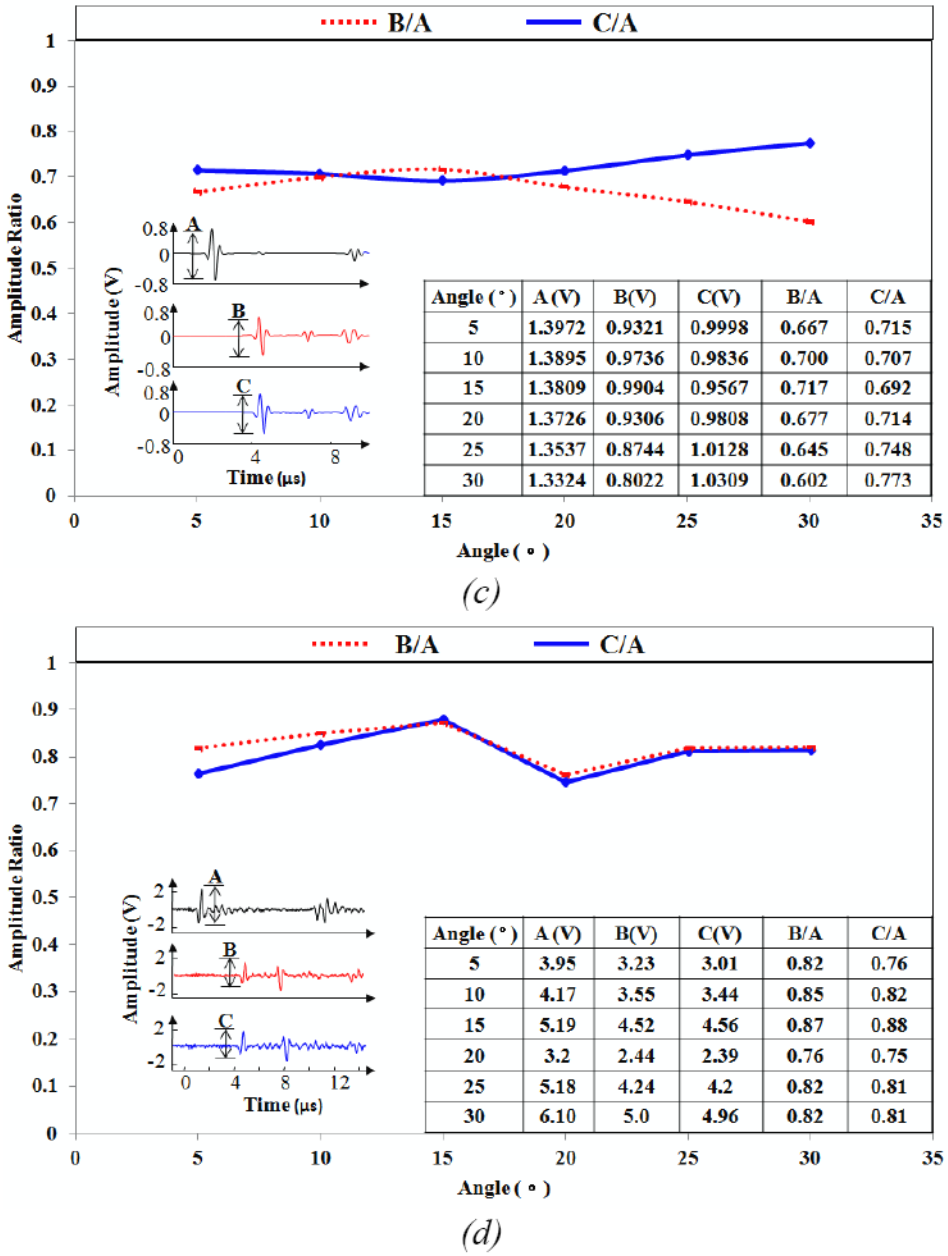

Angle (°)	A (V)	B(V)	C(V)	B/A	C/A
5	1.3972	0.9321	0.9998	0.667	0.715
10	1.3895	0.9736	0.9836	0.700	0.707
15	1.3809	0.9904	0.9567	0.717	0.692
20	1.3726	0.9306	0.9808	0.677	0.714
25	1.3537	0.8744	1.0128	0.645	0.748
30	1.3324	0.8022	1.0309	0.602	0.773

Angle (°)	A (V)	B(V)	C(V)	B/A	C/A
5	3.95	3.23	3.01	0.82	0.76
10	4.17	3.55	3.44	0.85	0.82
15	5.19	4.52	4.56	0.87	0.88
20	3.2	2.44	2.39	0.76	0.75
25	5.18	4.24	4.2	0.82	0.81
30	6.10	5.0	4.96	0.82	0.81

Figure 8.

Y-junction structure measurement. *(a)* Samples; *(b)* Measurement setup: Receive signals from different focal points, A: without passing junction, B: passing junction through branch with an angle, C: passing junction through straight line; *(c)* Simulation results of angle versus amplitude ratio. Inset: Representative signal shapes from junction with 15 degrees; and *(d)* Experimental results of angle versus amplitude ratio. Inset: Representative signal shapes from junction with 15 degrees.

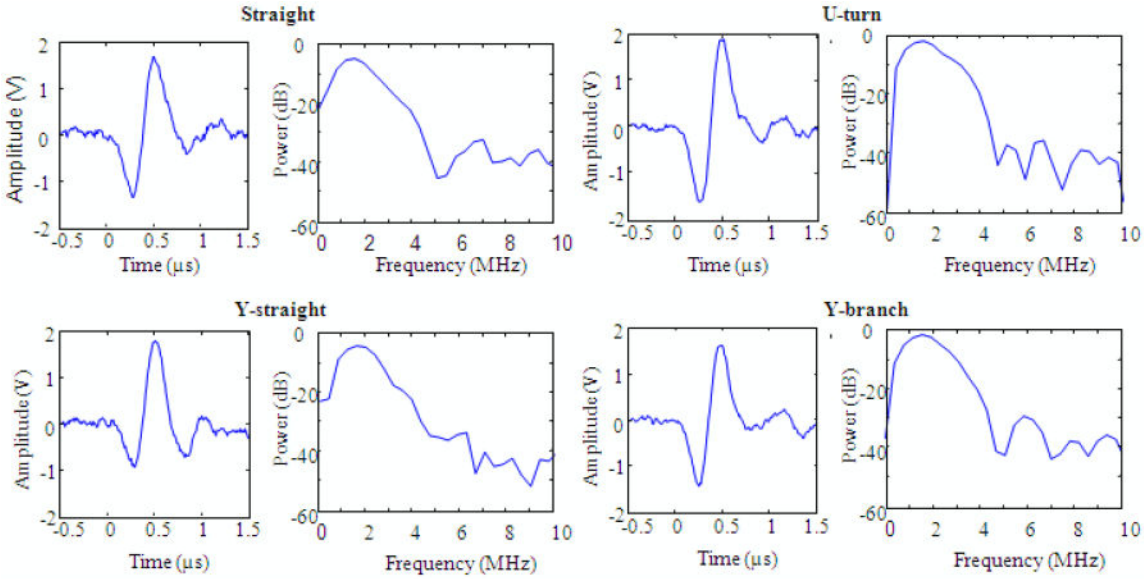

Figure 9.
Pulse shape and spectrum of different structures.

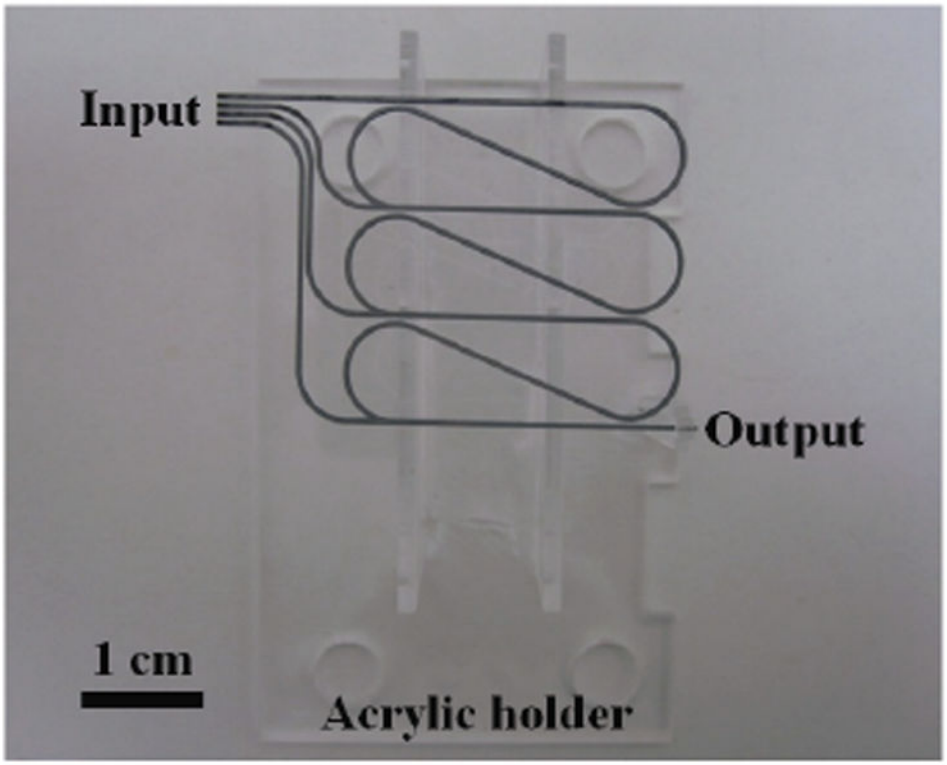

Figure 10.
4-channel serial delay lines assembled on an acrylic holder.

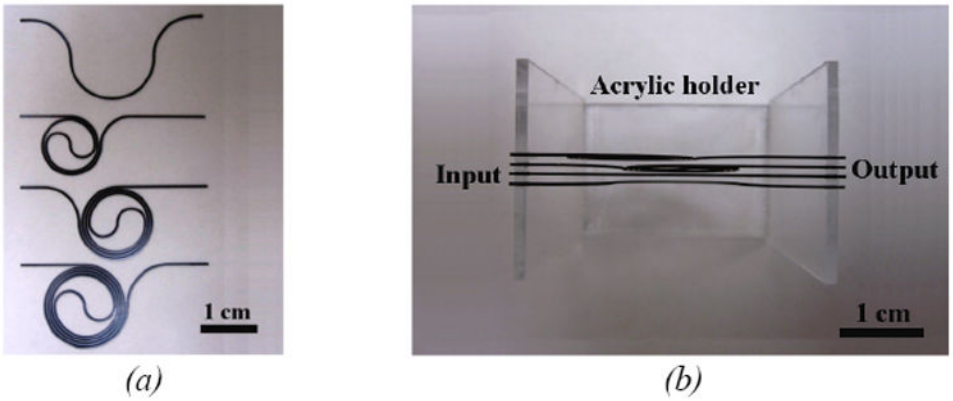

Figure 11.
4-channel parallel delay lines. *(a)* Fabricated; and *(b)* Assembled on an acrylic holder.

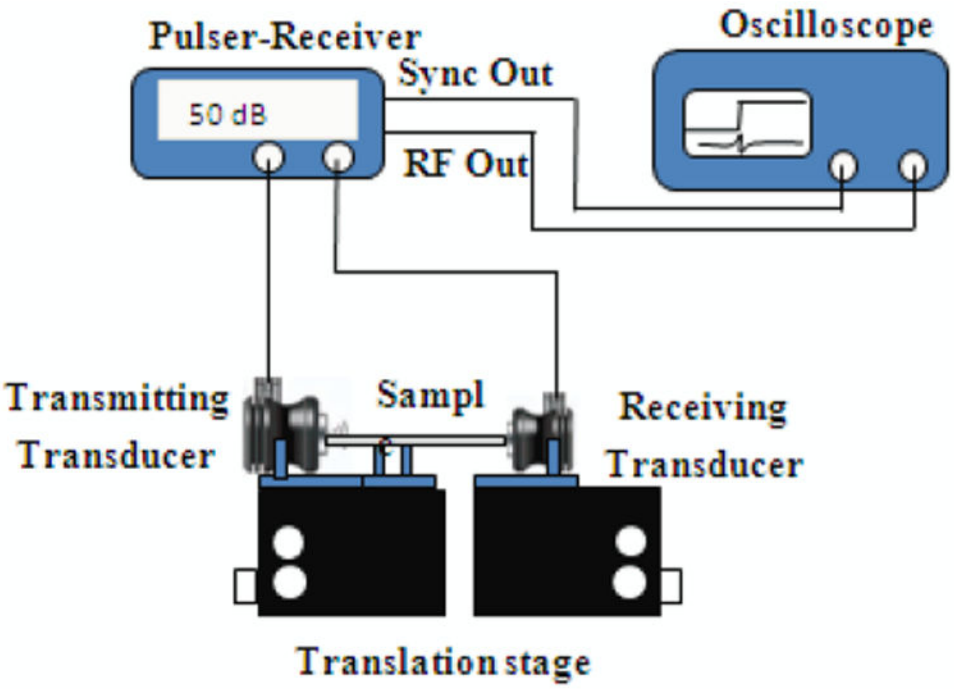

Figure 12.
Two-port through transmission setup.

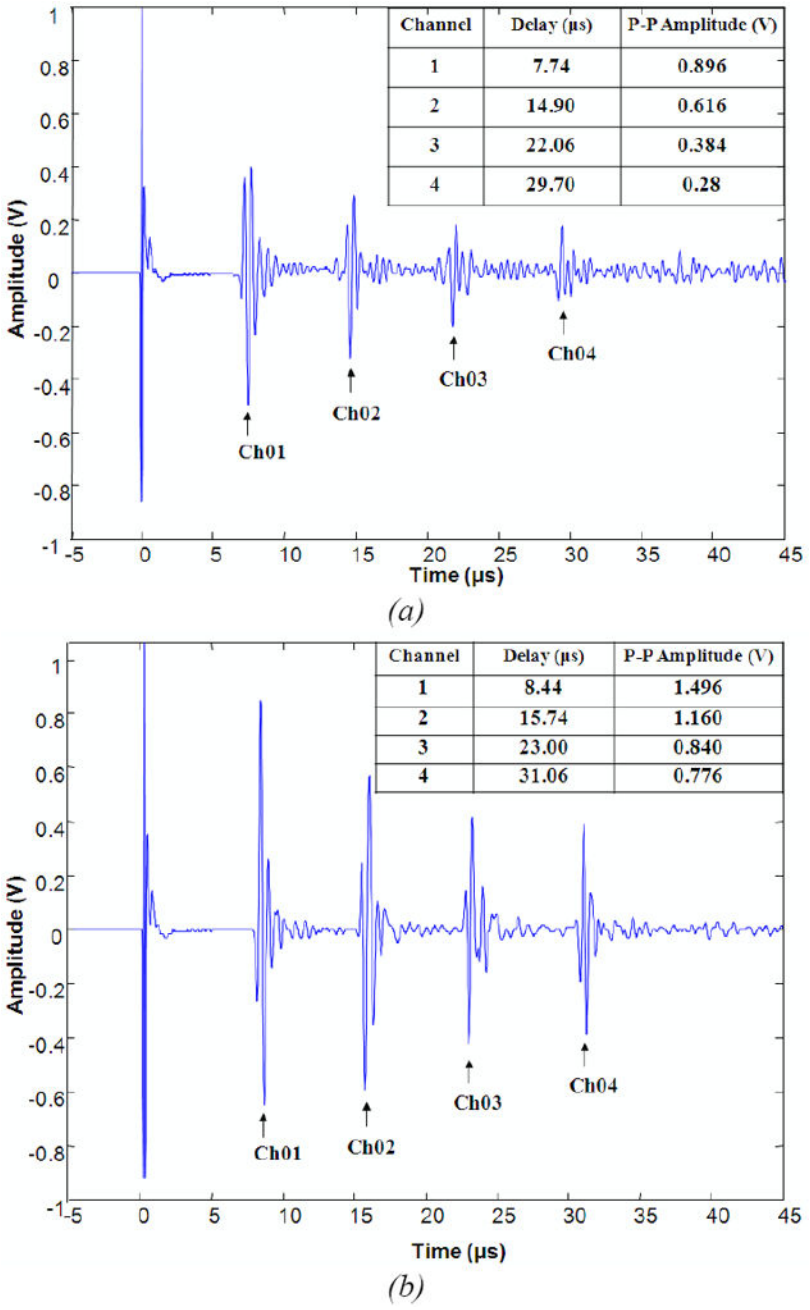

Figure 13.

Time-delayed signals from. *(a)* 4-channel serial delay lines; and *(b)* 4-channel parallel delay lines.